

Role of Microtearing Turbulence in DIII-D High Bootstrap Current Fraction Plasmas

X. Jian^{1,*}, C. Holland,¹ J. Candy,² E. Belli,² V. Chan,² A. M. Garofalo,² and S. Ding^{3,4}

¹University of California, San Diego, La Jolla, California 92093-0417, USA

²General Atomics, P.O. Box 85608, San Diego, California 92186-5608, USA

³Oak Ridge Associated Universities, Oak Ridge, Tennessee 37831, USA

⁴Institute of Plasma Physics, Chinese Academy of Sciences, P.O. Box 1126, Hefei, Anhui, 230031, China



(Received 7 June 2019; revised manuscript received 3 October 2019; published 26 November 2019)

We report on the first direct comparisons of microtearing turbulence simulations to experimental measurements in a representative high bootstrap current fraction (f_{BS}) plasma. Previous studies of high f_{BS} plasmas carried out in DIII-D with large radius internal transport barriers (ITBs) have found that, while the ion energy transport is accurately reproduced by neoclassical theory, the electron transport remains anomalous and not well described by existing quasilinear transport models. A key feature of these plasmas is the large value of the normalized pressure gradient, which is shown to completely stabilize conventional drift-wave and kinetic ballooning mode instabilities in the ITB, but destabilizes the microtearing mode. Nonlinear gyrokinetic simulations of the ITB region performed with the CGYRO code demonstrate that the microtearing modes are robustly unstable and capable of driving electron energy transport levels comparable to experimental levels for input parameters consistent with the experimental measurements. These simulations uniformly predict that the microtearing mode fluctuation and flux spectra extend to significantly shorter wavelengths than the range of linear instability, representing significantly different nonlinear dynamics and saturation mechanisms than conventional drift-wave turbulence, which is also consistent with the fundamental tearing nature of the instability. The predicted transport levels are found to be most sensitive to the magnetic shear, rather than the temperature gradients more typically identified as driving turbulent plasma transport.

DOI: [10.1103/PhysRevLett.123.225002](https://doi.org/10.1103/PhysRevLett.123.225002)

Introduction.—Electron energy transport in a magnetized plasma is still not a fully understood subject in magnetic fusion research [1]. Experimentally observed energy transport levels are far larger than that induced by collisional processes described by neoclassical theory [2]. Various drift-wave instabilities, such as the ion temperature gradient (ITG) mode, trapped electron mode (TEM), and electron temperature gradient (ETG) mode, have been proposed as mechanisms for driving the observed transport levels. Gyrofluid and gyrokinetic simulations of these instabilities have yielded impressive agreement with experimental observations in many [3–9], but not all [10], cases. More recently, multiscale simulations [11–13] have shown that strong nonlinear interactions may occur between different scale components of the turbulent system (ranging from $k_y \rho_s \sim 0.1$ to $k_y \rho_s \sim 100$, where $k_y = nq/r$, n , q , and r are the toroidal mode number, safety factor, and outboard midplane minor radius, respectively, and ρ_s the ion sound speed gyroradius) in the DIII-D ITER-baseline [14], Alcator C-Mod [15], and JET [16] plasmas. Specifically, it was found that the experimental fluxes could be reproduced only when cross-scale interactions among ITG, TEM, and ETG are included. In addition, it has been shown that microtearing modes (MTMs) can also drive substantial electron thermal transport in both spherical [17–19] and conventional tokamaks [4,20,21],

and they can also exhibit multiscale interactions with ETG modes [13].

DIII-D is a conventional aspect-ratio tokamak that aims to help establish the scientific basis for the optimization of the tokamak approach to fusion energy production. Scenarios with high bootstrap current [22] fraction ($f_{BS} = I_{BS}/I_p$), where I_{BS} is the spontaneously generated toroidal current induced by the pressure gradient under toroidal geometry [23] and I_p is the total plasma current, are desirable for steady-state or long-pulse operation of future reactors [24], as they can reduce the cost for auxiliary heating power. Building upon on the high f_{BS} scenario pioneered in JT-60U and other machines [24–29], the high f_{BS} scenario currently being developed in DIII-D [30–32] as an attractive candidate for future burning plasmas is characterized by a strong internal transport barrier (ITB) in almost all of the kinetic channels and a relatively high safety factor q ($q_{95} > 6$, where q_{95} denotes the value at the 95% poloidal flux surface).

One area of great interest is understanding which physical mechanism controls the ITB strength in this scenario. Transport analysis of high f_{BS} discharges on DIII-D shows that neoclassical transport often dominates the ion energy channel [30], while the mechanism(s) responsible for electron energy transport, which is far larger than predicted

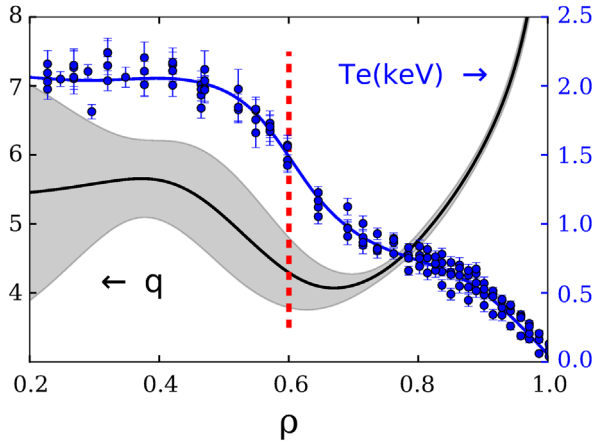


FIG. 1. Profiles of safety factor q and electron temperature T_e . The uncertainties of the q profile (indicated by the shaded region) are evaluated using a Monte Carlo analysis based upon diagnostic uncertainties.

by neoclassical theory, remain unclear. Analysis of earlier high f_{BS} discharges in JT-60U [33,34] and other machines relied upon older reduced transport models such as the CDBM [35] and GLF23 [36] models, which assume that the transport is driven by local ballooning-type instabilities but have a wide variety of restrictive simplifying assumptions and limitations regarding physics such as flow shear [33]. More recent transport modeling of DIII-D high f_{BS} discharges which used the trapped gyro-Landau fluid [37] model was unable to reproduce the inferred electron energy transport levels within the ITB [38], particularly at high safety factor q [32]. The DIII-D scenario typically has high toroidal $\beta_t = 2\mu_0 p/B_t^2$ and normalized value $\beta_N = \beta_t/(I_p/aB)$ [30] (2.5% and 3.3, respectively, for the case considered here), larger than the earlier JT-60U plasmas [26,39] and closer to the values expected in a future reactor. Here, p , B_t , and a are the plasma pressure, the toroidal magnetic field, and the value of r at the separatrix, respectively. In NSTX plasmas with dominant neoclassical ion transport and electron ITBs (but significantly lower q values than the high f_{BS} scenario of interest here), gyrokinetic modeling predicted that short-wavelength ETG turbulence should dominate [40].

Gyrokinetic Calculation.—In order to resolve this problem, a systematic gyrokinetic stability and transport analysis of the ITB region from a representative high f_{BS} discharge (shot number 176125 at 2600 ms) was performed. The specific radius considered is $\rho = 0.6$ (Fig. 1), which has $a/L_{T_e} = 4.1$ and $s = -0.8$. Here, ρ is the normalized toroidal flux, $a/L_{T_e} = -aT_e/\nabla T_e$, and s is the magnetic shear defined as $s = (r/q)(dq/dr)$. The kinetic profiles come from a dedicated profile fitting tool [41,42]. Additional parameters are listed in Table I, where R is the plasma torus major radius, ν_e is the collisionality defined as $\nu_e = (a/c_s)(\sqrt{2}\pi e^4 n_e/m_e^{1/2} T_e^{3/2}) \ln \Lambda$ [43], and c_s , m_e , and e are the ion sound speed, electron mass, and

TABLE I. Parameters of $\rho = 0.6$.

r/a	R/a	a/L_{T_e}	a/L_{T_i}	a/L_{n_e}	T_e/T_i
0.62	3.05	4.1	2.7	3.4	0.73
s	q	$\beta_{E,\text{unit}}$	α	γ_E	ν_e
-0.80	4.3	$5.9e-3$	3.9	0.082	0.14

electron charge, respectively. $\beta_{e,\text{unit}} = 8\pi n_e T_e/B_{\text{unit}}^2$, with B_{unit} being the effective field strength [44], and $\alpha = -q^2(\partial_r V/2\pi^2)(V/2\pi^2 R_0)^{1/2} 4\pi \partial_r P/(rB_{\text{unit}})^2 \approx -q^2 R \beta_e \nabla p/p$ in an infinite aspect-ratio shifted circle geometry [45], where V is the plasma volume. γ_E is the shearing rate of the radial electrical field (E_r) defined as $\gamma_E = -(a/c_s)(r/q)(\partial\omega_0/\partial r)$, where ω_0 is the toroidal rotation frequency contributed by the E_r .

Linear calculation using CGYRO [43] shows that the most common turbulent transport instability candidates, i.e., electrostatic drift waves (DW) ranging from $k_y \rho_s = 0.1$ to 100, which includes the typical ITG mode, TEM, and ETG mode, are all fully stabilized by the strong local Shafranov shift, which is proportional to α (hence also called α stabilization [46]). By systematically scaling the value of α in electrostatic stability analysis, it is found that, by 70% of the experimental α value, the TEM and ETG instabilities at this radius are stabilized [Fig. 2(a)], while the ITG mode is predicted to always be stable. More realistic electromagnetic calculations (which include both the perpendicular and transverse magnetic field fluctuations) find that the kinetic ballooning mode (KBM) is unstable for small values of α at long wavelengths, but it can similarly be fully stabilized at about half of the experimental α , leaving a stable gap at larger α . Interestingly, if we continue to increase α toward the experimental level, the MTM is eventually destabilized [Figs. 2(b) and 2(c)]. An additional test was performed in which a/L_n and a/L_T were

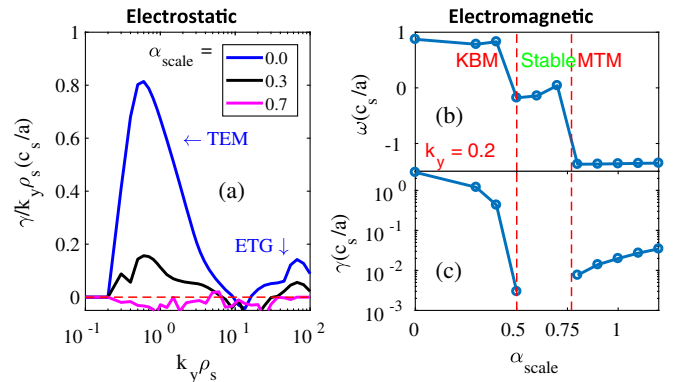


FIG. 2. (a) $\gamma/k_y \rho_s$ (where γ is the linear growth) of the electrostatic drift waves for different scaling factors of experimental α . The (b) frequency and (c) growth rate of dominant electromagnetic instability of $k_y \rho_s = 0.2$ versus α_{scale} .

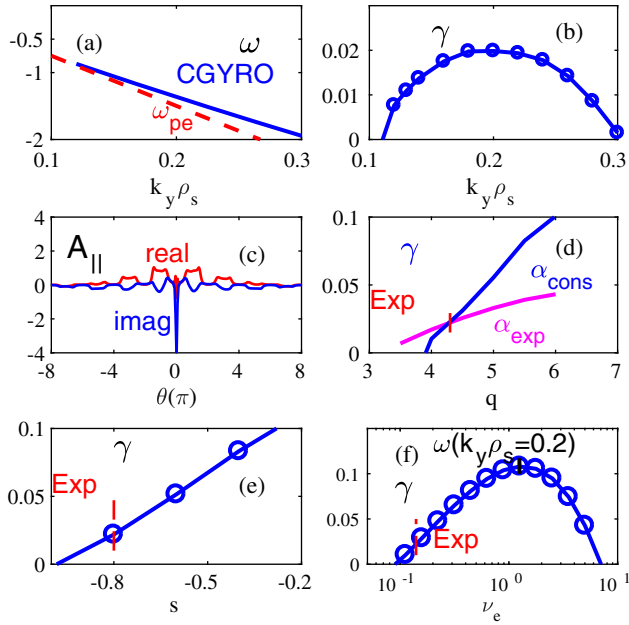


FIG. 3. The (a) frequency and (b) growth rate spectrum of the MTM. (c) The eigenfunction of A_{\parallel} ($k_y \rho_s = 0.2$) in the ballooning space. The growth rate of $k_y \rho_s = 0.2$ versus (d) q , (e) s , and (f) ν_e . “ α_{exp} ” and “ α_{cons} ” in (d) mean, respectively, that α is fixed to the experimental value and that it varies with q self-consistently.

respectively scaled down and up simultaneously while keeping the pressure gradient fixed, and it’s found that the ITG and ETG modes are not destabilized until η_i and $\eta_e \sim 4$ ($\eta_{i,e} = L_{n_e}/L_{T_{i,e}}$), respectively, far larger than the experimental values ($\eta_{i, \text{exp}} = 0.8$ and $\eta_{e, \text{exp}} = 1.2$). We note that (i) only the magnetic drift velocity (the geometry effect) is changed when the α scaling is performed, while the a/L_T and $\beta_{e, \text{unit}}$ are kept fixed, and (ii) nonlocal effects which might destabilize the KBM are not included.

In order to verify that the unstable mode is in fact a MTM, the scaling of the linear frequency, growth rate, and eigenfunction with key driving and damping parameters are shown in Fig. 3. The frequency is shown to be very close to $\omega_{p_e}^* = k_y \rho_s (a/L_{p_e})$ [Fig. 3(a)], consistent with MTM theory [47,48], and the mode is found to be unstable over the range of $k_y \rho_s = [0.1, 0.3]$ [Fig. 3(b)]. The eigenfunction of the parallel magnetic potential A_{\parallel} of $k_y \rho_s = 0.2$ is of tearing parity [Fig. 3(c)], which is another strong indication of MTM. The existence of a strong A_{\parallel} peak at $\theta = 0$ (where θ is the ballooning angle) has been carefully checked using a very high poloidal resolution to eliminate possible numerical errors. It is shown that both higher q [Fig. 3(d)] and lower $|s|$ [Fig. 3(e)] are efficient for MTM destabilization since they are favorable in expanding the current channel width, which both makes magnetic shielding more difficult, as first shown by Drake *et al.* [49], and reduces k_{\parallel} ($\propto k_y s/q$) so that field line bending stabilization is weakened. In addition, if α is varied self-consistently with q while the pressure gradient is kept fixed, the MTM can be

more sensitive to the value of q [Fig. 3(d), black line]. In addition, the mode’s growth rate depends nonmonotonically [50,51] on the collisionality, achieving a maximum value at $\nu_e \sim 1c_s/a$ [Fig. 3(f)], which is comparable to the real frequency and consistent with theoretical expectations for MTMs [48]. Most notably, our analysis indicates that at these parameters, the magnetic shear has the largest impact on the MTM growth rate (in terms of the fractional change in γ for the fractional change in the physics parameter).

With linear analysis showing that all of the ballooning type modes (including the ITG mode, TEM, ETG mode, and KBM) are stable and far from instability boundaries, only the MTM survives at the experimental parameters. These results indicate a clear inability of previously discussed reduced transport models to accurately predict the electron transport in the ITB region of these plasmas, as they rely upon ballooning-type modes being locally unstable. Furthermore, these plasma conditions provide an ideal setting for evaluating the capability of MTMs to drive experimentally relevant electron energy flux (Q_e) levels in the core of conventional aspect-ratio tokamaks. As noted in the Introduction, this question is particularly relevant for assessing our ability to accurately predict the structure of ITBs in future steady-state scenarios, where bootstrap currents driven by strong pressure gradients will play a much larger role in setting confinement and performance levels than inductive scenarios.

In order to assess the ability of MTMs to actually drive electron transport at levels consistent with an experiment (as inferred via power balance analysis performed with the TRANSP code [52]), a series of nonlinear spectral gyrokinetic simulations including extensive convergence tests were performed with the CGYRO code. Only key results of the simulations are reported in this Letter, with more extensive discussion deferred to a future publication. Our simulations used a 128-point velocity space grid (eight energies and 16 pitch angles). In configuration space, we use up to 48 poloidal grid points and a fifth order differencing scheme in the parallel direction, combined with 120 radial modes and 24 binormal modes. The mode numbers are chosen to have resolutions of $\Delta k_x \rho_s = 0.2$ and $\Delta k_y \rho_s = 0.08$ such that $(L_x, L_y) = (31\rho_s, 78\rho_s)$, where L_x and L_y are the radial and binormal lengths, respectively. $\Delta x/\rho_s \sim 0.25$ and $k_{x, \text{max}} \rho_s$ is 11.8, which is enough to resolve the fine structure of MTM turbulence. Three charged species (deuterium and carbon ions as well as electrons) are included, and magnetic shaping via a generalized Miller parametrization [53] is employed. Both the perpendicular and transverse magnetic perturbations are included. We use the Sugama model to describe collisional effects [54]. All simulations were performed on the CORI machine at NERSC, with 9216 cores used for a typical simulation. Each simulation required 24–48 h to complete, and approximately 8×10^6 core hours were used in total.

The time traces of the energy flux of each species for experimental parameters are shown in Fig. 4(a). A large

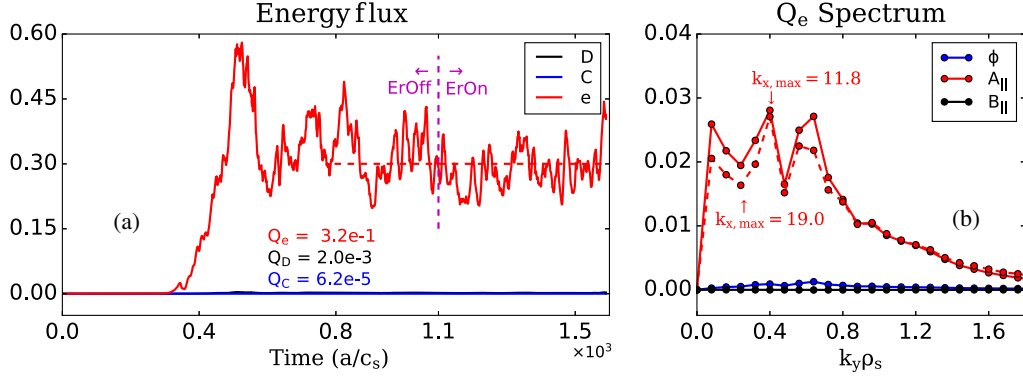


FIG. 4. (a) The trace traces of the gyro-Bohm normalized energy flux of different species; “D,” “C,” and “e” represent deuterium, carbon, and electrons, respectively. (b) The energy spectrum of Q_e induced by different fields. The results of $k_{x, \max} \rho_s$ equal to 11.8 and 19.0 are shown.

electron energy flux Q_e but near-zero ion energy flux Q_i is observed, which is consistent with the experimental analysis, after accounting for neoclassical transport. In addition, it is found that almost all of Q_e is driven by magnetic flutter [A_{\parallel} , Fig. 4(b)], in accordance with the linear analysis depicted in Fig. 2 and fitting expected MTM characteristics. Although the equilibrium E_r shearing rate is far larger than the MTM growth rate, it is found to have no effect on the predicted flux, as shown in Fig. 4(a) and consistent with the previous work [4,20]. An increase of the radial grid number by $\sim 60\%$ ($k_{x, \max} \rho_s$ of 19.0 in Fig. 4) yields a similar predicted flux spectrum, indicating good convergence in $k_{x, \max} \rho_s$. As described above, the MTM is the only linearly unstable mode for these parameters and is itself unstable only over the range $k_y \rho_s = 0.1-0.3$ [Fig. 3(b)], whereas the Q_e spectrum extends well beyond $k_y \rho_s = 1$. A similar phenomenon was observed in earlier MTM simulations by Doerk *et al.* [21]. We also note that the nonlinear excitation of linearly stable MTMs by linearly unstable ITG modes has been previously studied, by Hatch *et al.* [55], although the ITG (and other ballooning modes) are stable in this case. Developing a physics-based understanding of what sets the saturated MTM flux spectrum is crucial if a reliable reduced model of MTM transport suitable for use in future predictive transport modeling studies is to be developed. In this context, it remains to be determined whether the model of Rafiq *et al.* [56,57] can reproduce the predicted MTM flux and fluctuation spectra.

Sensitivity Study.—While this simulation demonstrates that the MTM drives finite values of Q_e but negligible values of Q_i for the experimental parameters, the predicted value $Q_{e, \text{sim}}/Q_{gB} = 0.32$ is several times lower than the experimentally inferred value of $Q_{e, \text{expt}}/Q_{gB} = 1.2$. Here, $Q_{gB} = n_e T_e c_s (\rho_s/a)^2$ [43]. However, experimental uncertainties must be accounted for in any meaningful comparisons between experiment and simulation, particularly gradient-driven turbulence simulations such as these.

In this Letter, we focus on assessing the impact of experimental uncertainties in the magnetic shear s on the results, motivated by the linear stability analysis shown in Fig. 3. The uncertainties of s corresponding to the nominal experimental q profile shown in Fig. 1 are shown in Fig. 5(a), and the corresponding variation in the linear growth rate spectra in Fig. 5(b). The fractional uncertainties in s are significantly larger than q due to the radial derivative inherent in the definition of s . Specifically, at $\rho = 0.6$, s is predicted to lie between -1.2 and -0.3 . The corresponding values of Q_e predicted by CGYRO for different values of s are shown in Fig. 5(c). Consistent with the linear analysis, Q_e significantly increases with weaker magnetic shear. In particular, the simulations match the experimentally inferred Q_e at $s = -0.3$, which is (barely) within the experimental uncertainties, although we also note that all other parameters have been held fixed, including key MTM drivers such as a/L_{Te}

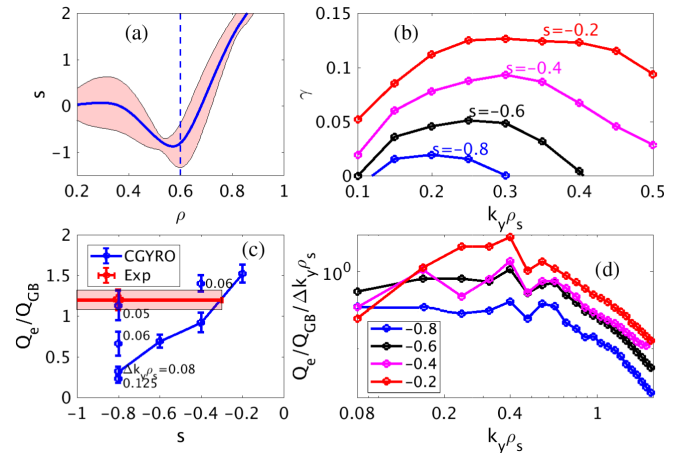


FIG. 5. (a) The s profile with uncertainties evaluated from Monte Carlo analysis. (b) Linear MTM spectra of different magnetic shear. (c) Comparison between the CGYRO predicted Q_e and the experimental one. (d) Variation of $Q_e(k_y)$ with s for $\Delta k_y \rho_s = 0.08$.

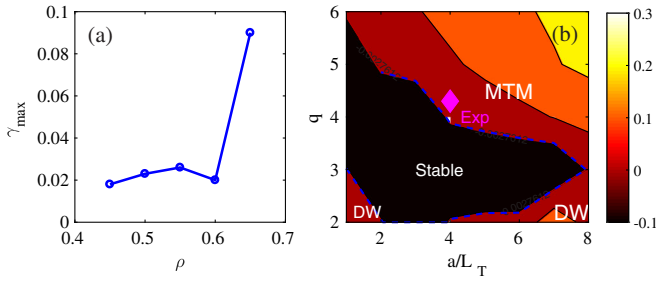


FIG. 6. (a) Maximum growth rate of MTM in the ITB region. (b) Contour plot of the growth rate of $k_y \rho_s = 0.2$ in the q and a/L_T space.

and ν_e . In addition, we note that all local ballooning-type instabilities are stable for the entire range of s considered due to the strong α stabilization and, therefore all of the fluxes shown in Fig. 5(c) are driven purely by MTMs.

Examination of the Q_e spectrum in Fig. 4(c) shows that significant contributions to the total flux come from values of $k_y \rho_s \leq 0.1$, where the MTMs are also linearly stable, which is consistent with some previous MTM theory [58] and modeling [18] studies. Additional studies in which the binormal simulation domain size L_y is increased (corresponding to a decrease in the minimum $k_y \rho_s$ value denoted by $\Delta k_y \rho_s$) find that the predicted values of Q_e increase as well, but with a minimum value of $Q_e/Q_{gB} \sim 0.3$, as shown in Fig. 5(c). We note that a value of $k_y \rho_s = 0.04$ corresponds to toroidal mode number $n = 1$, so further increases in L_y would not be physical. Moreover, we find that the Q_e magnitude and spectral shape depend sensitively upon the value of s used, likely reflecting the strong dependence of the linear growth rate spectrum on s [Fig. 5(d)]. In particular, at $s = -0.3$, where the $\Delta k_y \rho_s = 0.08$ simulations best match the experimental flux, the Q_e spectrum peaks at $k_y \rho_s = 0.4$. A fuller exploration of this issue will be presented in future work; here, we seek only to emphasize that only the MTMs generate electron energy fluxes consistent with the experimentally inferred levels and parameters.

Additional linear analysis indicates that the MTM dominates across the whole ITB region, from $\rho = 0.45$ to $\rho = 0.65$, with maximum growth rate vs radius plotted in Fig. 6(a). The remarkable increase in growth rate at $\rho = 0.65$ compared to $\rho = 0.6$ comes mainly from the weaker magnetic shear there, while all of the other background parameters are similar, which is consistent with Fig. 3(e). So-called nonlocal effects could alter the linear growth rates, although the size and magnitude of their impact are difficult to quantify. In order to identify the conditions under which MTM would dominate, a linear scan of $k_y \rho_s = 0.2$ over the q and a/L_T space was performed (assuming that $L_{T_e} = L_{T_i}$) based on the background parameters of $\rho = 0.6$ [Fig. 6(b)]. As can be seen, the DW and MTM instabilities separately dominate at low and high q , respectively. The reason for this

is that higher q leads to a strong Shafranov shift, which is favorable for α stabilization of DW, while increasing α and weakening k_{\parallel} due to higher q contribute to MTM destabilization, which is consistent with Fig. 3(d). Findings shown in Fig. 6 indicate that MTM may be routinely destabilized in the high f_{BS} scenario and would likely be responsible for regulating the electron pressure profile in the ITB region. Future work will extend this analysis to scenarios currently being developed for next-generation devices such as ITER.

Conclusion.—Identifying the mechanism’s driving electron transport in core ITBs when the ion thermal transport is neoclassical remains an important open problem in tokamak research. In this Letter, we have demonstrated convincingly for the first time that MTMs are *uniquely* able to drive the inferred levels of electron transport in the ITB region of a typical high f_{BS} DIII-D plasma, which is a candidate scenario for future tokamak reactors. Gyrokinetic analysis finds that all other local ballooning-type instabilities, including the ITG mode, TEM, ETG mode, and KBM, are strongly stabilized for these conditions by the large local Shafranov shift α which, on the other hand, destabilizes the MTMs. Relative to previous studies of high f_{BS} plasmas in machines such as JT-60U [39], the DIII-D plasmas have higher β and α , which we have shown here can significantly impact the dominant instability. These results present a strong challenge for predictive core transport models based purely upon conventional ballooning instabilities and inspire the further development and validation of such models to include MTM physics. In particular, these simulations predict that significantly different fluctuation characteristics should be observed than would be expected if local ballooning modes are responsible for driving the transport. More broadly, these findings generalize the conclusions of other recent transport studies [4,59], which identify MTMs as a “mode of last resort” in controlling the structure of transport barriers from edge to core, and therefore, to the whole plasma, when conventional instabilities are suppressed by mechanisms such as α stabilization or E_r shear.

Our discussions with W. Guttenfelder, D. R. Hatch, M. J. Pueschel, and M. Kotschenreuther are greatly appreciated. Assistance from M. Q. Wu for the equilibrium reconstruction is also appreciated. This work was supported by the U.S. Department of Energy under Awards No. DE-SC0018287, No. DE-SC0017992, No. DE-FG02-95ER54309, and No. DE-FC02-04ER54698. This research used resources of the National Energy Research Scientific Computing Center (NERSC), a U.S. Department of Energy Office of Science User Facility operated under Contract No. DE-AC02-05CH11231.

The views and opinions of authors expressed herein do not necessarily state or reflect those of the U.S. Government or any agency thereof.

*Corresponding author.
xijian@ucsd.edu

- [1] D. Batchelor *et al.*, Simulation of fusion plasmas: Current status and future direction, *Plasma Sci. Technol.* **9**, 312 (2007).
- [2] R. Hawryluk *et al.*, Fusion plasma experiments on TFTR: A 20 year retrospective, *Phys. Plasmas* **5**, 1577 (1998).
- [3] C. Holland, Validation metrics for turbulent plasma transport, *Phys. Plasmas* **23**, 060901 (2016).
- [4] D. Hatch, M. Kotschenreuther, S. Mahajan, P. Valanju, F. Jenko, D. Told, T. Görler, and S. Saarelma, Microtearing turbulence limiting the JET-ILW pedestal, *Nucl. Fusion* **56**, 104003 (2016).
- [5] S. J. Freethy, T. Görler, A. J. Creely, G. D. Conway, S. S. Denk, T. Happel, C. Koenen, P. Hennequin, and A. E. White, Validation of gyrokinetic simulations with measurements of electron temperature fluctuations and density-temperature phase angles on ASDEX Upgrade, *Phys. Plasmas* **25**, 055903 (2018).
- [6] A. Creely *et al.*, Validation of nonlinear gyrokinetic simulations of L- and I-mode plasmas on Alcator C-Mod, *Phys. Plasmas* **24**, 056104 (2017).
- [7] J. Citrin, H. Arnichand, J. Bernardo, C. Bourdelle, X. Garbet, F. Jenko, S. Hacquin, M. J. Pueschel, and R. Sabot, Comparison between measured and predicted turbulence frequency spectra in ITG and TEM regimes, *Plasma Phys. Controlled Fusion* **59**, 064010 (2017).
- [8] P. Rodriguez-Fernandez *et al.*, Perturbative transport modeling of cold-pulse dynamics in Alcator C-Mod Ohmic plasmas, *Nucl. Fusion* **59**, 066017 (2019).
- [9] H. Doerk, A. Bock, A. Di Siena, E. Fable, T. Görler, F. Jenko, and J. Stober, Turbulence in high-beta ASDEX upgrade advanced scenarios, *Nucl. Fusion* **58**, 016044 (2018).
- [10] C. Holland, A. E. White, G. R. McKee, M. W. Shafer, J. Candy, R. E. Waltz, L. Schmitz, and G. R. Tynan, Implementation and application of two synthetic diagnostics for validating simulations of core tokamak turbulence, *Phys. Plasmas* **16**, 052301 (2009).
- [11] J. Candy, R. Waltz, M. Fahey, and C. Holland, The effect of ion-scale dynamics on electron-temperature-gradient turbulence, *Plasma Phys. Controlled Fusion* **49**, 1209 (2007).
- [12] S. Maeyama, Y. Idomura, T.-H. Watanabe, M. Nakata, M. Yagi, N. Miyato, A. Ishizawa, and M. Nunami, Cross-Scale Interactions Between Electron and Ion Scale Turbulence in a Tokamak Plasma, *Phys. Rev. Lett.* **114**, 255002 (2015).
- [13] S. Maeyama, T.-H. Watanabe, and A. Ishizawa, Suppression of Ion-Scale Microtearing Modes by Electron-Scale Turbulence via Cross-Scale Nonlinear Interactions in Tokamak Plasmas, *Phys. Rev. Lett.* **119**, 195002 (2017).
- [14] C. Holland, N. Howard, and B. Grierson, Gyrokinetic predictions of multiscale transport in a DIII-D ITER baseline discharge, *Nucl. Fusion* **57**, 066043 (2017).
- [15] N. Howard, C. Holland, A. White, M. Greenwald, and J. Candy, Multi-scale gyrokinetic simulation of tokamak plasmas: Enhanced heat loss due to cross-scale coupling of plasma turbulence, *Nucl. Fusion* **56**, 014004 (2016).
- [16] N. Bonanomi, P. Mantica, J. Citrin, T. Goerler, and B. Teaca, Impact of electron-scale turbulence and multi-scale interactions in the JET tokamak, *Nucl. Fusion* **58**, 124003 (2018).
- [17] K. L. Wong, S. Kaye, D. R. Mikkelsen, J. A. Krommes, K. Hill, R. Bell, and B. LeBlanc, Microtearing Instabilities and Electron Transport in the NSTX Spherical Tokamak, *Phys. Rev. Lett.* **99**, 135003 (2007).
- [18] W. Guttenfelder, J. Candy, S. M. Kaye, W. M. Nevins, E. Wang, R. E. Bell, G. W. Hammett, B. P. LeBlanc, D. R. Mikkelsen, and H. Yuh, Electromagnetic Transport from Microtearing Mode Turbulence, *Phys. Rev. Lett.* **106**, 155004 (2011).
- [19] D. Dickinson, C. M. Roach, S. Saarelma, R. Scannell, A. Kirk, and H. R. Wilson, Microtearing modes at the top of the pedestal, *Plasma Phys. Controlled Fusion* **55**, 074006 (2013).
- [20] H. Doerk, F. Jenko, T. Görler, D. Told, M. J. Pueschel, and D. R. Hatch, Gyrokinetic prediction of microtearing turbulence in standard tokamaks, *Phys. Plasmas* **19**, 055907 (2012).
- [21] H. Doerk, F. Jenko, M. Pueschel, and D. Hatch, Gyrokinetic Microtearing Turbulence, *Phys. Rev. Lett.* **106**, 155003 (2011).
- [22] O. Sauter, C. Angioni, and Y. Lin-Liu, Neoclassical conductivity and bootstrap current formulas for general axisymmetric equilibria and arbitrary collisionality regime, *Phys. Plasmas* **6**, 2834 (1999).
- [23] W. Houlberg, K.-C. Shaing, S. Hirshman, and M. Zarnstorff, Bootstrap current and neoclassical transport in tokamaks of arbitrary collisionality and aspect ratio, *Phys. Plasmas* **4**, 3230 (1997).
- [24] C. Gormezano *et al.*, Steady state operation, *Nucl. Fusion* **47**, S285 (2007).
- [25] T. Fujita *et al.*, High performance reversed shear plasmas with a large radius transport barrier in JT-60U, *Nucl. Fusion* **38**, 207 (1998).
- [26] T. Fujita *et al.*, Quasisteady High-Confinement Reversed Shear Plasma with Large Bootstrap Current Fraction Under Full Noninductive Current Drive Condition in JT-60U, *Phys. Rev. Lett.* **87**, 085001 (2001).
- [27] T. Fujita, Spatial structure of internal and edge transport barriers, *Plasma Phys. Controlled Fusion* **44**, A19 (2002).
- [28] Y. Sakamoto, T. Fujita, S. Ide, A. Isayama, M. Takechi, T. Suzuki, H. Takenaga, N. Oyama, Y. Kamada, and (The JT-60 Team), Stationary high confinement plasmas with large bootstrap current fraction in JT-60U, *Nucl. Fusion* **45**, 574 (2005).
- [29] Y. Sakamoto *et al.*, Characteristics of internal transport barriers in JT-60U reversed shear plasmas, *Nucl. Fusion* **41**, 865 (2001).
- [30] A. M. Garofalo *et al.*, Compatibility of internal transport barrier with steady-state operation in the high bootstrap fraction regime on DIII-D, *Nucl. Fusion* **55**, 123025 (2015).
- [31] S. Ding *et al.*, Confinement improvement in the high poloidal beta regime on DIII-D and application to steady-state H-mode on EAST, *Phys. Plasmas* **24**, 056114 (2017).
- [32] J. McClenaghan *et al.*, Transport modeling of the DIII-D high scenario and extrapolations to ITER steady-state operation, *Nucl. Fusion* **57**, 116019 (2017).
- [33] N. Hayashi, J. Garcia, M. Honda, E. Narita, S. Ide, G. Giruzzi, and Y. Sakamoto, Transport modelling of JT-60U and JET plasmas with internal transport barriers towards prediction of JT-60SA high-beta steady-state scenario, *Nucl. Fusion* **57**, 126037 (2017).

- [34] J. Garcia, N. Hayashi, B. Baiocchi, G. Giruzzi, M. Honda, S. Ide, P. Maget, E. Narita, M. Schneider, and H. Urano, Physics comparison and modelling of the JET and JT-60U core and edge: Towards JT-60SA predictions, *Nucl. Fusion* **54**, 093010 (2014).
- [35] K. Itoh, S.-I. Itoh, A. Fukuyama, M. Yagi, and M. Azumi, Self-sustained turbulence and L-mode confinement in toroidal plasmas. II, *Plasma Phys. Controlled Fusion* **36**, 1501 (1994).
- [36] R. E. Waltz, G. M. Staebler, W. Dorland, G. W. Hammett, M. Kotschenreuther, and J. A. Konings, A gyro-Landau-fluid transport model, *Phys. Plasmas* **4**, 2482 (1997).
- [37] G. Staebler, J. Kinsey, and R. Waltz, A theory-based transport model with comprehensive physics, *Phys. Plasmas* **14**, 055909 (2007).
- [38] C. Pan, G. M. Staebler, L. L. Lao, A. M. Garofalo, X. Gong, Q. Ren *et al.*, Investigation of energy transport in DIII-D High- β_p EAST-demonstration discharges with the TGLF turbulent and NEO neoclassical transport models, *Nucl. Fusion* **57**, 036018 (2017).
- [39] Y. Kamada, Extended JT-60U plasma regimes for high integrated performance, *Nucl. Fusion* **41**, 1311 (2001).
- [40] J. L. Peterson, R. Bell, J. Candy, W. Guttenfelder, G. W. Hammett, S. M. Kaye, B. LeBlanc, D. R. Mikkelsen, D. R. Smith, and H. Y. Yuh, Suppressing electron turbulence and triggering internal transport barriers with reversed magnetic shear in the National Spherical Torus Experiment, *Phys. Plasmas* **19**, 056120 (2012).
- [41] N. Logan, B. A. Grierson, S. R. Haskey, S. P. Smith, O. Meneghini, and D. Eldon, OMFIT tokamak profile data fitting and physics analysis, *Fusion Sci. Technol.* **74**, 125 (2018).
- [42] O. Meneghini *et al.*, Integrated modeling applications for tokamak experiments with OMFIT, *Nucl. Fusion* **55**, 083008 (2015).
- [43] J. Candy, E. Belli, and R. Bravenec, A high-accuracy Eulerian gyrokinetic solver for collisional plasmas, *J. Comput. Phys.* **324**, 73 (2016).
- [44] J. Candy, A unified method for operator evaluation in local Grad-Shafranov plasma equilibria, *Plasma Phys. Controlled Fusion* **51**, 105009 (2009).
- [45] R. Waltz and R. Miller, Ion temperature gradient turbulence simulations and plasma flux surface shape, *Phys. Plasmas* **6**, 4265 (1999).
- [46] M. A. Beer, G. W. Hammett, G. Rewoldt, E. J. Synakowski, M. C. Zarnstorff, and W. Dorland Gyrofluid simulations of turbulence suppression in reversed-shear experiments on the Tokamak Fusion Test Reactor, *Phys. Plasmas* **4**, 1792 (1997).
- [47] J. Drake and Y. Lee, Kinetic theory of tearing instabilities, *Phys. Fluids* **20**, 1341 (1977).
- [48] R. D. Hazeltine, D. Dobrott, and T. Wang, Kinetic theory of tearing instability, *Phys. Fluids* **18**, 1778 (1975).
- [49] J. Drake, T. Antonsen, Jr., A. Hassam, and N. Gladd, Stabilization of the tearing mode in high-temperature plasma, *Phys. Fluids* **26**, 2509 (1983).
- [50] D. Carmody, M. Pueschel, and P. Terry, Gyrokinetic studies of microinstabilities in the reversed field pinch, *Phys. Plasmas* **20**, 052110 (2013).
- [51] I. Predebon and F. Sattin, On the linear stability of collisionless microtearing modes, *Phys. Plasmas* **20**, 040701 (2013).
- [52] R. Hawryluk, in *Physics of Plasmas Close to Thermonuclear Conditions* (Elsevier, New York, 1981), pp. 19–46.
- [53] R. Miller, M. Chu, J. Greene, Y. Lin-Liu, and R. Waltz, Noncircular, finite aspect ratio, local equilibrium model, *Phys. Plasmas* **5**, 973 (1998).
- [54] H. Sugama, T.-H. Watanabe, and M. Nunami, Linearized model collision operators for multiple ion species plasmas and gyrokinetic entropy balance equations, *Phys. Plasmas* **16**, 112503 (2009).
- [55] D. R. Hatch, M. J. Pueschel, F. Jenko, W. M. Nevins, P. W. Terry, and H. Doerk, Origin of Magnetic Stochasticity and Transport in Plasma Microturbulence, *Phys. Rev. Lett.* **108**, 235002 (2012).
- [56] T. Rafiq, J. Weiland, A. Kritz, L. Luo, and A. Pankin, Microtearing modes in tokamak discharges, *Phys. Plasmas* **23**, 062507 (2016).
- [57] T. Rafiq, A. Kritz, J. Weiland, L. Luo, and E. Schuster, Study of the parametric dependence of linear and nonlinear microtearing modes in conventional tokamak discharges, *Phys. Plasmas* **25**, 012504 (2018).
- [58] J. Drake, N. Gladd, C. Liu, and C. Chang, Microtearing Modes and Anomalous Transport in Tokamaks, *Phys. Rev. Lett.* **44**, 994 (1980).
- [59] M. Kotschenreuther *et al.*, Gyrokinetic analysis, and simulation of pedestals, to identify the culprits for energy losses using “fingerprints”, *Nucl. Fusion* **59**, 096001 (2019).